AGU Advances

RESEARCH ARTICLE
10.1029/2019AV000161

Key Points:
- High-resolution observations illustrate the vast lateral extent and cross-wake variability in upper ocean mixing caused by hurricane passage
- Observed changes in ocean mixed layer depths are impacted by salinity and are closely approximated by a mixing depth parameterization
- Cold wake observations yield insights relevant to short-term (intensification) and long-term (ocean heat storage) hurricane impacts

Supporting Information:
- Supporting Information S1
- Original Version of Manuscript
- Peer Review History
- Authors' Response to Peer Review Comments
- First Revision of Manuscript [Accepted]

Correspondence to:
E. R. Sanabia,
sanabia@usna.edu

Citation:
Sanabia, E. R., & Jayne, S. R. (2020). Ocean observations under two major hurricanes: Evolution of the response across the storm wakes. *AGU Advances*, *1*, e2019AV000161. https://doi.org/10.1029/2019AV000161

Received 31 DEC 2019
Accepted 18 MAY 2020

Peer Review
The peer review history for this article is available as a PDF in the Supporting Information.

Ocean Observations Under Two Major Hurricanes: Evolution of the Response Across the Storm Wakes

Elizabeth R. Sanabia[1] **and Steven R. Jayne**[2]

[1]Oceanography Department, United States Naval Academy, Annapolis, MD, USA, [2]Physical Oceanography Department, Woods Hole Oceanographic Institution, Woods Hole, MA, USA

Abstract Hurricanes fundamentally alter the upper ocean thermal structure across millions of square kilometers annually through a medley of complex processes that are not well understood but are critically important to hurricane intensification. High-resolution, air-deployed profiling float observations beneath Hurricanes Irma (2017) and Florence (2018) detail storm-induced changes in upper ocean temperature, salinity, and density structures. This unique and comprehensive data set allows for validation and quantification of results from previous observational and modeling studies, including the time evolution of sea surface cooling and upper ocean near-inertial oscillations, greater mixed layer deepening right of each storm track, and inhibition of mixing by salinity stratification (beneath Irma). These observations also reveal that storm-forced upper ocean currents remain remarkably uniform with increasing distance from the radius of maximum winds and result in consistent mixed layer deepening, particularly right of each storm track. These observed ocean mixed layer depth changes are closely approximated by a mixing depth parameterization, which may enhance storm-forced ocean response predictability and therefore increase hurricane intensity forecast accuracy. Further, these hurricane-induced upper ocean temperature changes contribute to the evolving nature of hurricanes and ocean heat storage on seasonal and climate time scales.

Plain Language Summary Hurricanes cool the oceans along their paths as strong winds forcefully mix warm tropical surface waters with cooler waters below, creating a cold wake behind each storm. Hurricanes require very warm surface waters to develop and strengthen; therefore, cold wakes are important because they can affect storm intensity. Detailed ocean observations within a hurricane environment are rare but are needed to verify and quantify physical processes that govern cold wake development and decay and to accurately predict hurricane intensity. We used new instruments called Air Launched Autonomous Micro Observer floats to measure the cold wakes in two major Atlantic hurricanes: Irma (2017) and Florence (2018). Float measurements across each storm track revealed that, while ocean conditions prior to each storm were different, the hurricanes caused the upper oceans to cool in similar ways. We found that ocean temperature changes created by these strong hurricane winds could be predicted reasonably well using a formula developed a decade ago. We also found that our salinity measurements were necessary to use this formula accurately. This result is important because predicting ocean temperature changes can help weather forecasters accurately predict hurricane intensity and help climate scientists understand the impacts of hurricanes on heat storage in the world's oceans.

1. Introduction

Results from leading tropical cyclone (TC) coupled forecast models identify the need for increased ocean observations to improve hurricane intensity forecast accuracy (Chen, Cummings, et al., 2017; Mogensen et al., 2017). Observations are required ahead of the storm to establish initial conditions and beneath and behind the storm to improve parameterizations related to upper ocean mixing and air-sea fluxes, which are critical factors affecting near-surface atmospheric circulation and therefore hurricane intensification (Bell et al., 2012; Green & Zhang, 2013). Moreover, hurricane-forced mixing alters the upper ocean thermal structure across millions of square kilometers annually. The formation of a cold wake behind TCs has been documented as far back as the early 1940s (Suda, 1943) and is a well-known feature of the observed air-sea

interaction with TCs (e.g., D'Asaro et al., 2007; Fisher, 1958; Leipper, 1967; Mrvalijevic et al., 2013). Understanding the dynamics of cold wake formation processes has evolved from upwelling of cold subsurface waters (Hidaka & Akiba, 1955) to include entrainment mixing processes driven by surface currents (Elsberry et al., 1976) and refined to elucidate the particular role of enhanced shear-driven mixing induced by inertial currents in the upper ocean (Price, 1981), which remains widely accepted today. This shear-driven mixing is known to depend on upper ocean stratification (Chan et al., 2001; Price, 2009; Price et al., 1994; Sanford et al., 2007), which is particularly relevant to cold wake formation in regions where strong salinity gradients impede mixing during TC passage (e.g., Balaguru et al., 2018; Rudzin et al., 2018; Wang et al., 2011).

Climate studies routinely point out that changes in ocean temperatures contribute to the evolving nature of not only hurricanes (Bhatia et al., 2019; Emanuel, 2005; Holland & Bruyère, 2014; Murakami et al., 2018) but also sea life habitats (Lin, 2012; Walker et al., 2005) and ocean heat storage (Sriver & Huber, 2007) on seasonal (and longer) time scales (Dare & McBride, 2011). High-resolution ocean observations beneath major hurricanes are rare except during focused field programs (e.g., the Coupled Boundary Layer Air-Sea Transfer experiment, see Black et al., 2007; the Impact of Typhoons on the Ocean in the Pacific experiment, see D'Asaro et al., 2014), primarily due to the harsh and mostly inaccessible nature of the storm environment. While measuring ocean characteristics under hurricanes is a challenging endeavor, doing so is essential to improve hurricane forecast accuracy and to understand the changes hurricanes create in the world's oceans.

Here, the evolution of the upper ocean during the passage of two major Atlantic hurricanes is captured in exceptional spatial and temporal detail across each storm track with identical instrumentation, enabling detailed analyses of ocean processes below each storm as well as an intercomparison of upper ocean responses in regions with different initial conditions. In September 2017, eight Air Launched Autonomous Micro Observer (ALAMO) floats (Jayne & Bogue, 2017) were deployed from U.S. Air Force WC-130J "Hurricane Hunter" aircraft at 0.25° cross-track spacing and began recording observations about 20 hr prior to the arrival of Hurricane Irma, a Category-5 storm (Cangialosi et al., 2018). The floats were deployed across and centered on Hurricane Irma's westbound track (Figures 1 and S1 in the supporting information) nearly 500 km ahead of the TC and about 300 km east of the Lesser Antilles. One year later and 1,550 km to the northwest, nine ALAMO floats were deployed from another U.S. Air Force WC-130J at about 0.20° resolution across the forecast track of Hurricane Florence (Figures 1 and S1) and recorded observations beginning about 21 hr and over 600 km ahead of the approaching Category-4 storm (Stewart & Berg, 2019).

In both cases, the ALAMO floats profiled to near 300-m depth about every 2 hr, collecting temperature, salinity, and pressure measurements as each hurricane passed over the floats within 6 hr of maximum intensity (Cangialosi et al., 2018; Stewart & Berg, 2019; Figure S2). Observations collected prior to the arrival of outer wind bands permitted calculation of prestorm ocean conditions at each float location, which served as a basis for comparison to the ocean state during and after the passage of each storm. These initial conditions at the two array locations and the ocean response to each TC enable our analysis of changes in the upper ocean resulting from the passage of these major hurricanes.

Hurricane intensity is reliant upon the availability and transfer of energy from the ocean to the atmosphere. There is a strong negative feedback between the intensity of a TC and the cold ocean wake that it creates, as cooling sea surface temperatures (SSTs) reduce surface enthalpy fluxes into the hurricane (Cione & Uhlhorn, 2003). Further, the wake location, extent, and magnitude create unique asymmetries in enthalpy fluxes and result in force imbalances that alter the near-surface atmospheric circulation in ways that have given contradictory results in numerical studies, either decreasing (Chen, Elsberry, et al., 2017; Zhu et al., 2004) or increasing (Lee & Chen, 2014) hurricane intensity. Theoretical studies have shown that changes in upper ocean temperatures beneath a storm are driven mostly by mixing (D'Asaro et al., 2007) and that the mixing process is highly dependent on both the stress imparted to the ocean surface by the storm winds and the density stratification in the upper ocean under the storm (Price, 2009; Price et al., 1994). The interdependence of these air-sea interactions and importance of ocean cooling led to the implementation of the first operational coupled ocean-atmosphere hurricane forecast model nearly two decades ago (Bender et al., 2019). Accounting for the ocean response within

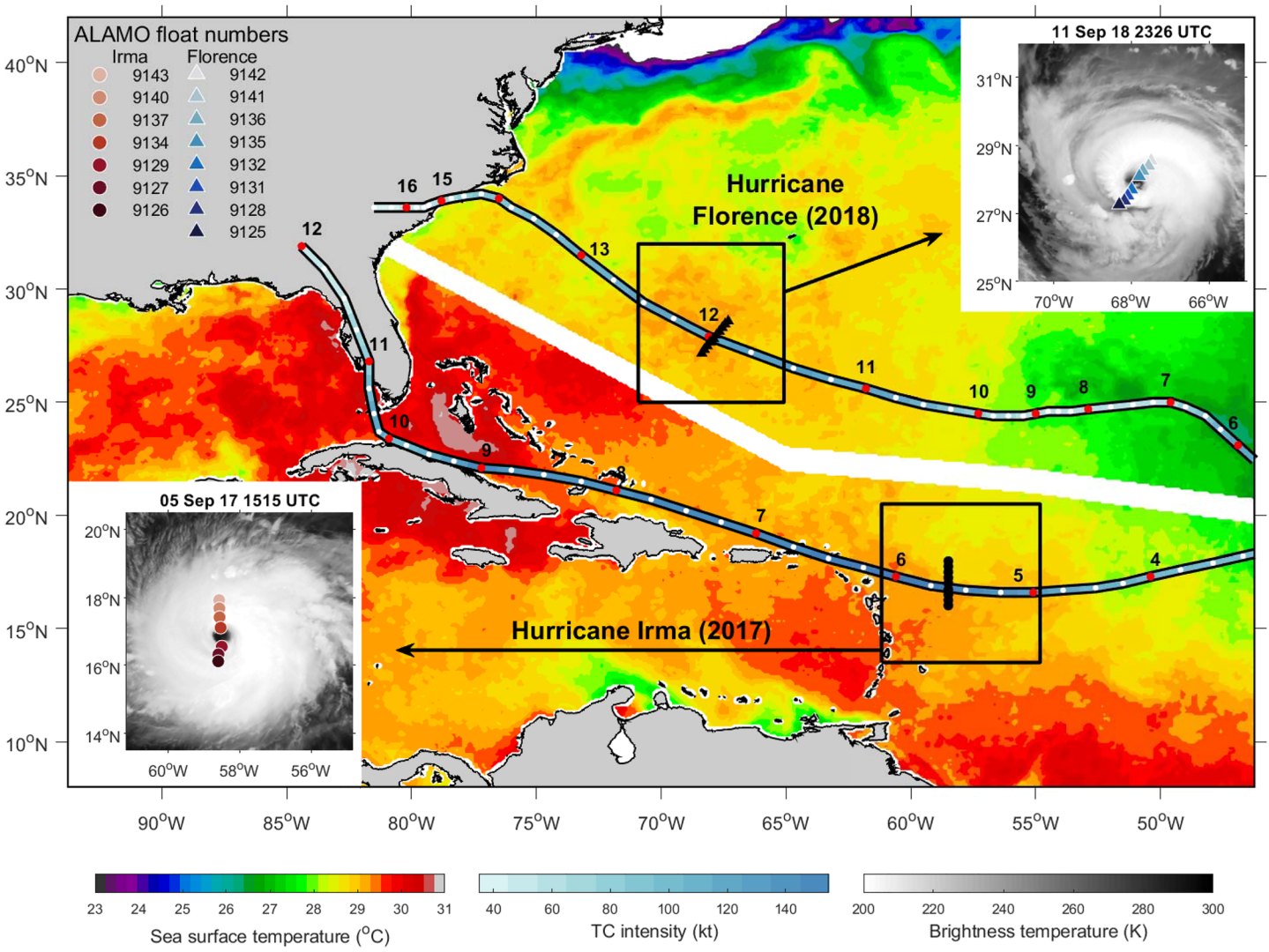

Figure 1. Prestorm sea surface temperatures and ALAMO float locations along each TC track. Prestorm satellite-derived SSTs (°C, shaded) and ALAMO float locations during Hurricanes Irma (2017, black circles) and Florence (2018, black triangles). Prestorm SSTs are from 2 September 2017 (Irma) and 8 September 2018 (Florence) to the southwest and northeast of the white break line, respectively. Storm intensities (kt) are shaded in blue along each hurricane track. Dates (black numbers) denote NHC best track positions at 0000 UTC (red dots); other synoptic hours (0600, 1200, and 1800 UTC) are marked by white dots. Black squares outline the locations of inset satellite IR brightness temperatures (K), and red circles (Irma) and blue triangles (Florence) mark ALAMO positions as each TC crossed the respective array.

hurricane forecast models has since been shown to improve intensity forecast skill (Halliwell et al., 2015; Mogensen et al., 2017).

2. Data and Methods

In situ measurements of temperature, salinity, and pressure from the ALAMO floats provide a time evolution of the density structure beneath each passing storm (processing specifics are detailed in the supporting information). The stress imparted to the ocean scales as the square of the surface wind speed (Edson et al., 2013), which is measured across each TC by the Stepped Frequency Microwave Radiometer (SFMR; Uhlhorn et al., 2007) aboard the aircraft. Upper ocean currents resulting from the wind stress are estimated from drift measurements derived from the ALAMO float surface position data (see supporting information). Taken together, these observations enable an evaluation of the mixing that is critical to understanding changes in the upper ocean structure, as well as surface heat exchange and hurricane intensification.

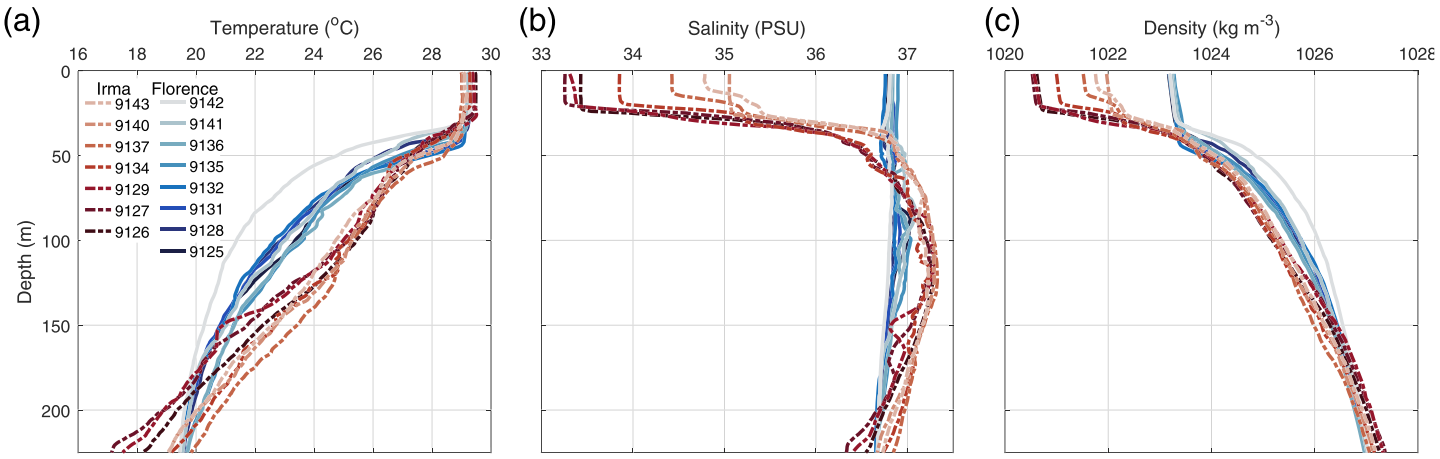

Figure 2. Mean pre-TC upper ocean conditions. (a) Temperature (°C), (b) salinity (PSU), and (c) density (kg m^{-3}) profiles for each ALAMO float prior to Hurricanes Irma (dashed red lines) and Florence (solid blue lines).

3. Results

3.1. Prestorm Ocean Conditions

Satellite measurements provide a large-scale view of SSTs (Figure 1) 3 days prior to the arrival of each hurricane over the respective ALAMO array (Wentz et al., 2000). Temperatures were similar, about 29°C at each array location. These satellite-measured SSTs matched the ALAMO float pre-TC measurements (Figure 2a), where 29°C temperatures extended to a depth of about 40 m, below which differences between each array location emerged. Between 50 and 200 m, temperatures at the Irma array were warmer than those along the Florence array, with a maximum difference of about 2.3°C near 120 m. The 26°C isotherm depths reflected this subsurface disparity, as upper ocean temperatures exceeded 26°C to an average of 79 m along the Irma array compared to 55 m along the Florence array.

Unlike temperatures, salinities varied widely in the upper 40 m (Figure 2b). Across the Irma array surface salinities were low, spanning 33.3–35.1 PSU, consistent with climatological values of the Amazon-Orinoco River plumes (Androulidakis et al., 2016; Ffield, 2007; Rudzin et al., 2019). Along the Florence array, surface waters were saltier (averaging 36.8 PSU) and spanned a much smaller range (0.14 PSU), also consistent with typical values (Androulidakis et al., 2016). Salinity differences across the arrays varied to a depth of about 50 m, below which salinities at the Irma array slightly exceeded those across the Florence array until about 200 m and by a maximum of about 0.4 PSU near 120 m. Greatest density differences were present in the upper 40 m, both across the Irma array and between the Irma and Florence arrays (Figure 2c). In the Irma array, greatest densities were on the northern side of the array, consistent with higher salinity values present farther from the Amazon-Orinoco River outflow region. The densities between 50 and 200 m for both arrays were broadly similar. Note that the upper ocean density differences would have been undetectable with temperature-only measurements, which illustrates the importance of salinity measurements for correctly initializing ocean models. In TCs, these measurements are particularly important, as density stratification determines stability and mixing of the water column. Further, variations in temperature and salinity mixed layer depths have been shown in both observational (Grodsky et al., 2012) and numerical (Hlywiak & Nolan, 2019; Rudzin et al., 2018) studies to result in barrier layers that impede mixing below TCs and thereby enhance intensification.

Prestorm satellite-derived surface currents in each region (Bonjean & Lagerloef, 2002) indicate the presence of relatively weak eddies across each float array prior to TC passage (Figure S3). Float surface velocities in the prestorm environment were similar to the satellite-derived currents and averaged 0.16 m s^{-1} across the Irma array and 0.12 m s^{-1} across the Florence array.

3.2. Hurricane Winds Over the Ocean Surface

Surface wind speeds across Irma and Florence (Figure 3) were measured by the SFMR aboard tasked hurricane reconnaissance aircraft while passing the ALAMO arrays. Each ALAMO float profile closest to the TC

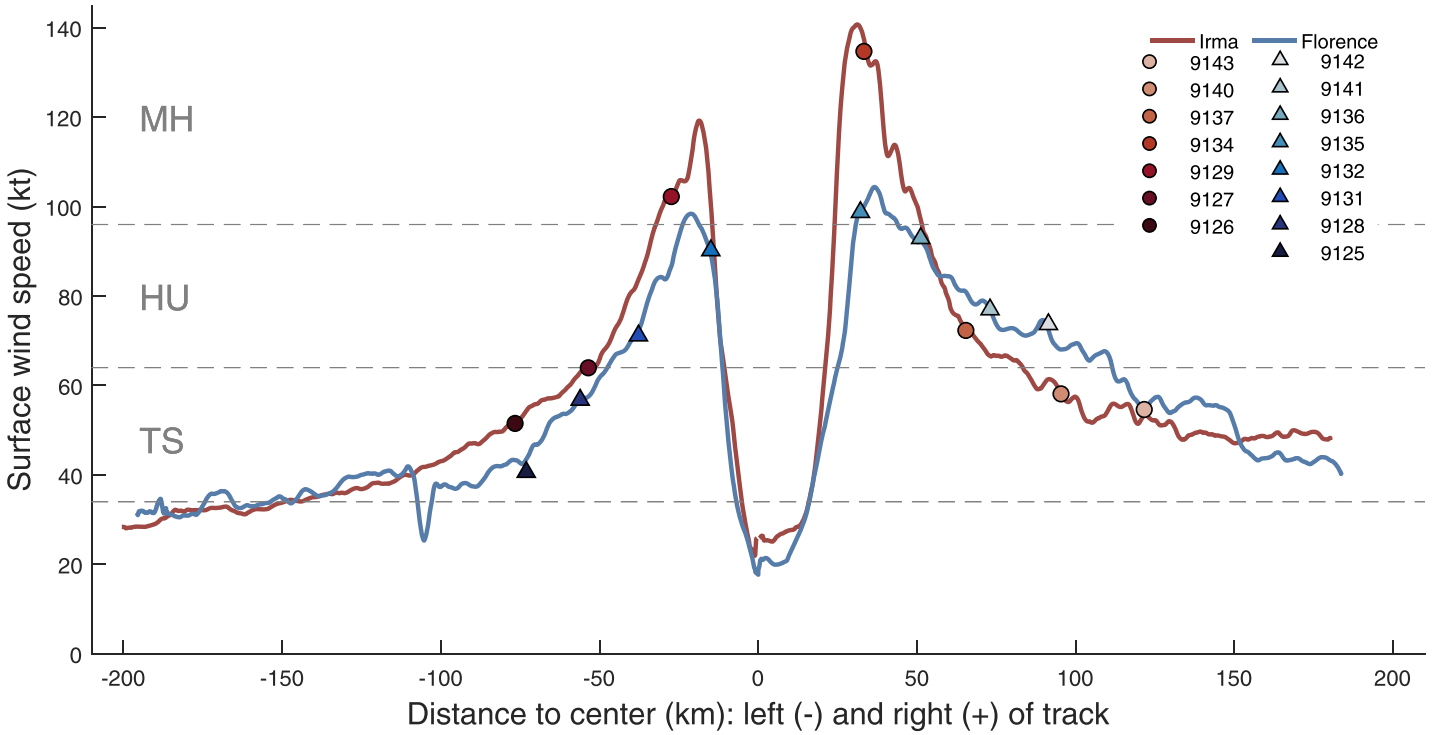

Figure 3. Surface wind speeds (kt) across Hurricanes Irma (red) and Florence (blue) as measured by the SFMR during the aircraft pass closest to each ALAMO array. The radial distance (km) and surface wind speed (kt) are shown for the closest location of each float to the TC center.

center was recorded within 1.5 hr of the aircraft transect (implying the winds in Figure 3 are a good representation of the winds acting at the sea surface as the ALAMOs collected ocean data). The ALAMOs were spaced similarly across the diameter of each hurricane—extending from about 75 km left to about 122 km right of the storm center. The closest float to either TC (9132) passed 15 km left of the Florence center, within the radius of maximum winds and therefore twice beneath the left eyewall. In both hurricanes, profiles were collected within 33 km left and right of the TC center—beneath each eyewall—meaning that ocean observations were collected beneath the strongest wind bands on both sides of these major hurricanes. Highest winds were recorded during profiles in Floats 9134 (135 kt in Irma) and 9135 (100 kt in Florence), 33 km to the right of each TC center. Wind speeds at the float profile locations varied as each TC crossed the respective array, from tropical storm (at five floats), to hurricane (at seven floats), to major hurricane (at three floats) intensity, indicating that the forcing imparted to the ocean at the float locations varied greatly. Relative differences in wind speed were also present across each track. Left of each center, wind speeds over the Irma floats were higher than over the Florence floats; however, right of center beyond the eyewall, wind speeds in Irma decayed more rapidly than in Florence and were lower at the outer float locations.

Both hurricanes moved across the ALAMO arrays at similar translation speeds (Figure S2): Irma at ~7 m s^{-1} and Florence at ~7.6 m s^{-1}, which indicates that the ~400-km diameter of these SFMR wind profiles would cross each array in less than 16 hr. During the 4-hr span of peak winds (at radii within 50 km), storm intensities varied by less than 5 kt, indicating the SFMR pass closest to the floats is sufficient to represent the winds at the float locations. Also, at these translation speeds, mixing would likely be the dominant physical process in the upper ocean at the float locations, as there is insufficient time for upwelling to become significant (Price, 1981; Samson et al., 2009).

3.3. Ocean Response

Ocean surface cooling in a TC wake is often noted in satellite SST measurements (Stramma et al., 1986), and that broadscale cooling is visible along the tracks of both Irma and Florence (Figures 4a and 4b). In both

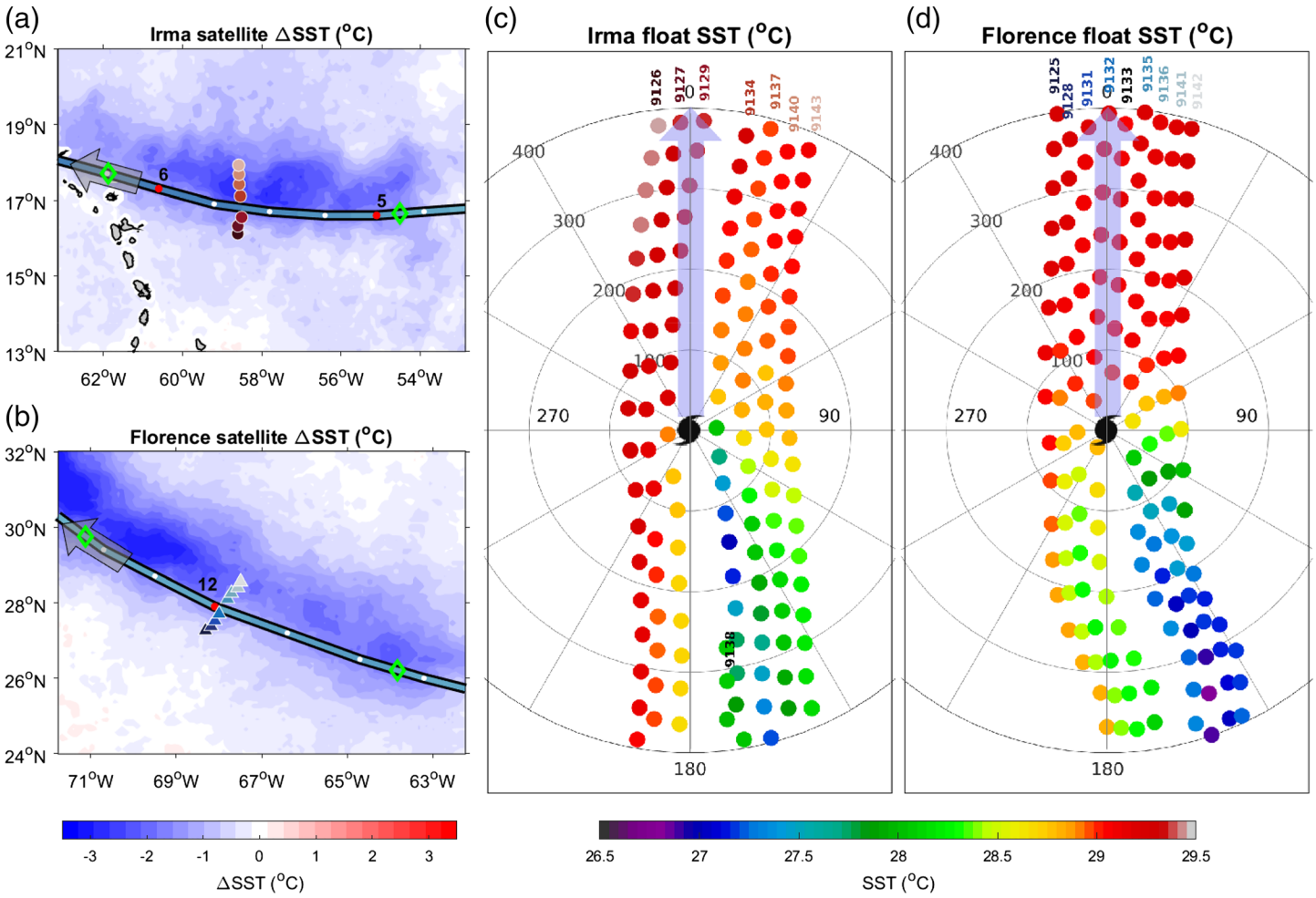

Figure 4. Ocean surface cooling during hurricane passage. Satellite-derived SST differences (°C) between the days following and preceding hurricane passage over the (a) Irma and (b) Florence ALAMO float arrays. Floats colored as in Figures 1–3; TC track as in Figure 1; green diamonds outline TC locations 400 km prior to and following array passage, corresponding to observation times in (c) and (d). The ALAMO float SST (°C) observations within 400 km of Hurricanes Irma (c) and Florence (d) in a storm-centered, storm-relative framework. Float numbers are adjacent to the first observation within 400 km of the TC center. Shaded arrows identify the direction of storm motion.

cases, greater cooling was present right of the TC track. Narrowing focus to the SST evolution along each ALAMO array, more details emerge. Placing each SST measurement relative to the TC center and heading at the observation time (Figures 4c and 4d) facilitates analysis of SST changes during hurricane passage. As the TCs approached the float locations, SSTs were near 29°C (consistent with prestorm conditions) and varied less than 0.5°C and 0.2°C across the Irma and Florence arrays, respectively. In both cases, greatest cooling compared to pre-TC conditions was observed behind and right of the TC centers, 2.3°C at Float 9134 in Irma and 2.4°C at Float 9136 in Florence. In Irma, SST cooling decayed radially outward, reaching only 1.0°C at the outermost float, while in Florence, the surface at all floats right of track cooled by at least 2.0°C. This post-TC cooling also greatly increased the range of SSTs across the wake (to 2.2°C in Irma and 2.0°C in Florence) compared to prestorm conditions.

Evaluating wind and sea conditions at individual float locations over time facilitates additional cross-track comparisons. Surface winds at each float location extrapolated from the closest SFMR transect across each storm (Figure 3) are shown at 1-hr increments (Figures 5a, S5, and S6, black vectors) and highlighted at the closest point of approach (CPA) of the TC center (Figures 5a, S5, and S6, red vectors). The magnitude and direction of the surface winds over each float changed as the hurricane approached (Figures 5a, S5, and S6). Magnitudes increased with proximity to the radius of maximum winds and were greatest at the

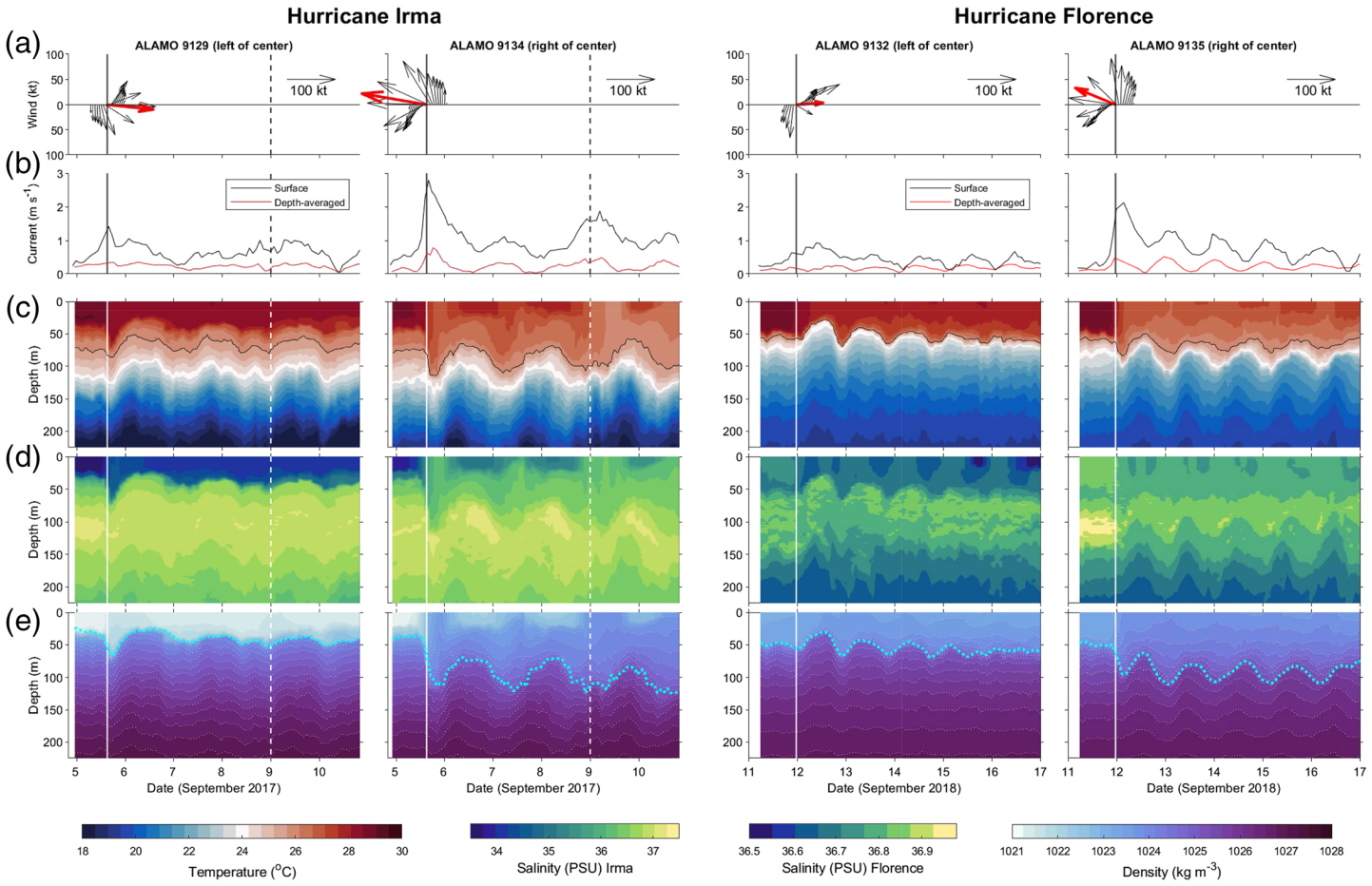

Figure 5. Eyewall ALAMO float observations before, during, and after hurricane passage. (a) Surface wind speed (kt) and direction (north up) at eyewall floats in Hurricanes Irma (columns 1 and 2) and Florence (columns 3 and 4) from aircraft SFMR observations (black vectors are hourly; red vectors denote winds at TC center CPA to float). (b) Sea surface (black line) and depth-averaged (red line) current speeds (m s^{-1}) derived from float GPS positions. (c) Temperature (°C, shaded) and 26°C isotherm (black line). (d) Salinity (PSU, shaded; note different scales for each storm). (e) Density (kg m^{-3}, shaded) and depth of maximum Brunt-Väisälä frequency (dotted cyan line). Solid vertical lines indicate the passage of each TC; dashed vertical lines indicate passage of Hurricane Jose over the Irma array.

storm CPA to the float, except in 9132, where CPA winds were bounded by higher values due to the float location within the eye of the storm. Wind direction varied on either side of each TC center. Right of track, winds rotated clockwise (Floats 9134 and 9135; Figure 5a), in the same direction as inertial motion (in the Northern Hemisphere), while left of track, they turned counterclockwise (Floats 9129 and 9132; Figure 5a), opposing inertial motion. Thus, the winds right of track resonantly excited strong inertial oscillations in the surface currents, while those left of track did not (Price, 1981; Samson et al., 2009).

These cross-track differences were also evident in the sea surface and layer-averaged horizontal current magnitudes derived from the float positions. In both cases, currents at the eyewall float locations were larger on the right side of the TC center (9134 and 9135) than on the left (9129 and 9132; Figure 5b); however, from the eyewall floats outward, the currents were remarkably similar—in stark contrast to the spatial variation in the storm-driven wind speeds present at the sea surface (Figures S5a, S5b, S6a, and S6b). At every location, the strongest surface currents were observed at or just after hurricane passage.

Impacts of these changing surface winds and currents on the upper ocean at the float locations are clear in vertical cross sections of temperature, salinity, and density over time. Conditions in the upper 225 m at the floats closest to each eyewall are depicted in Figures 5c–5e and at all float locations in Figures S5c–S5e and S6c–S6e. Similar to the SSTs, little variability was present in the subsurface ocean conditions prior to the arrival of each TC. This relative quiescence (noted by near-horizontal contour lines in Figures 5c–5e) was clearly

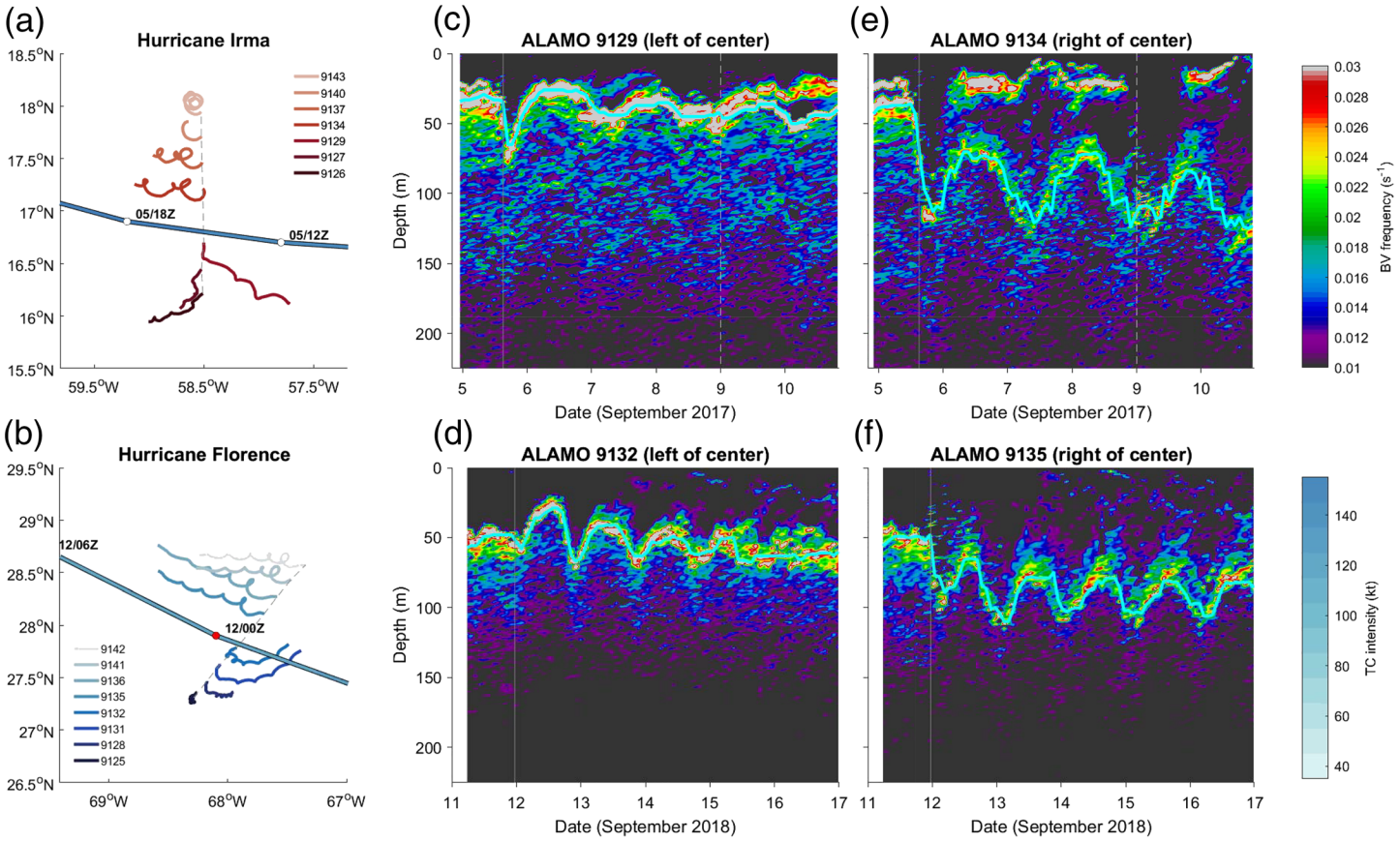

Figure 6. Float trajectories in Hurricanes (a) Irma and (b) Florence from deployment (dashed black line) through 5 days after TC passage. Buoyancy frequency (s^{-1}) for eyewall floats (c and d) left and (e and f) right of track. Depths (m) of maximum buoyancy frequency (cyan lines) are as in Figure 5.

disrupted by the hurricane passage over each array (solid vertical lines, Figure 5). Conditions began to change as the winds ahead of each TC reached the floats and continued for about 12 hr as the eye passed over the array (1505 UTC 05 September 2017 for Irma and 2325 UTC 11 September 2018 for Florence). Beneath the strong surface winds and currents, rapid deepening is evident in temperature, salinity, and density contours at most float locations (Figures 5c–5e, S5c–S5e, and S6c–S6e), particularly right of track. Similar deepening has been noted in a few cases previously (D'Asaro et al., 2007; Sanford et al., 2011; Shay et al., 1992) and is explained as shear-driven mixing when TC translation speeds exceed 4 m s^{-1} (Price, 1981), as is the case here.

Physically, the deepening contours indicate downward mixing of warmer, fresher surface waters well into the thermocline and halocline. Greatest deepening occurred right of each storm center, where, for example, the 26°C isotherm (black lines, Figure 5c) deepened 26 m in Irma (9134) and 21 m in Florence (9135), compared to changes of less than 10 m in the floats left of each TC center. Radially outward from the eyewall float locations, results were similar (Figures S5c and S6c), with greater deepening of the 26°C isotherm right-of-track (averaging 16 m in Irma and 24 m in Florence) than left-of-track (5 m in Irma and 7 m in Florence). Similar hurricane-forced changes were evident in upper ocean salinity, as fresher surface waters mixed downward into the saltier waters in the halocline more so on the right side of the TC than the left (Figure 5d; note that different scales were required to delineate salinity characteristics in each TC). These left-to-right (cross-track) differences were also evident in density cross sections (Figures 5e, S5e, and S6e) with greater descent of the isopycnals during the forcing phase occurring right of each TC center.

Once the TCs passed each array, the winds abated (Figure 5a), surface currents weakened (Figure 5b), and isopleth deepening ceased (Figures 5c–5e). Contours throughout the upper 200 m then heaved upward as internal waves generated by the wind forcing oscillated at near-inertial frequencies with amplitudes that

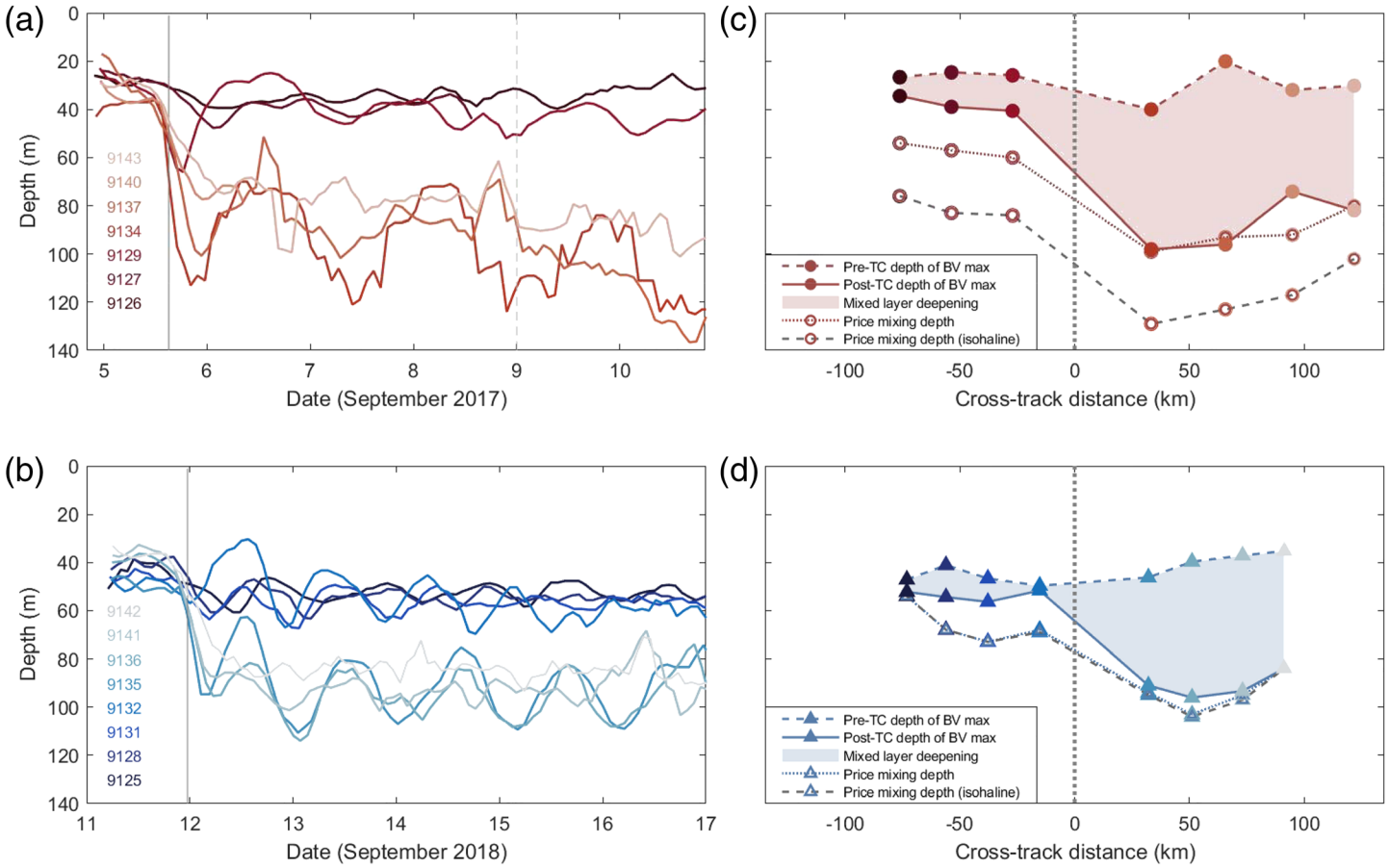

Figure 7. Ocean mixed layer deepening following hurricane passage. Depths (m) of maximum buoyancy frequency at (a) Irma and (b) Florence ALAMO float locations. Profile (*x* axes) and TC passage (vertical lines) times are as in Figure 5. (c and d) Mean depths (m) across the (c) Irma and (d) Florence ALAMO arrays of maximum buoyancy frequency before (dashed) and after (solid) TC passage and of mixing depths (m) from Price (2009) calculated for observed conditions (dotted) and with salinity held constant (dashed gray). Shading highlights observed mixed layer deepening across each array. Radial distances (km, *x* axes) denote float locations closest to TC center (as in Figure 3).

varied with wind magnitude (Figures 5c–5e). These oscillations are a well-known response to TC forcing (Geisler, 1970; Gill, 1984; Greatbatch, 1983; Price, 1983), occur in three dimensions, and are evident in the horizontal motion of the float surface trajectories (Figures 6a and 6b), as well as in the vertical cross sections (Figures 5c–5e), where inertial periods averaged 41.0 hr along the Irma array (near 17°N) and 25.6 hr along the Florence array (near 28°N). While the frequencies of these internal waves were similar, the amplitudes were not; they were greatest at the eyewall float locations and decreased radially outward from the TC center (Figures 5, S5, and S6). In most floats, the oscillations continued through the 5 days immediately following TC passage, although the response in the Irma floats was clearly reinvigorated by the passage of Hurricane Jose across the array 3.5 days after Irma (dashed vertical lines, Figures 5 and S5).

To better understand the evolution of mixing during the passage of both TCs, upper ocean stratification is measured through the Brunt-Väisälä (BV) frequency (see supporting information). The greater the BV frequency, the more highly stratified the parcel is and the more mechanical energy that is required to mix across it. Hence, mixing is most often present at low BV frequencies and less (or not) present at higher values. The depth of the maximum BV frequency is often therefore used as an indicator of the base of the mixed layer above the stratified ocean interior. This is illustrated for the eyewall floats in Figures 6c–6f and is plotted over density contours in Figure 5e. Examining the mixed layer depths at the float locations over time gives insight into the variability of storm-induced mixing across the TC track. Following TC passage, mixed layer depths (maximum BV frequency depths in cyan lines, Figure 5e) are deeper than in the pre-TC state in both storms, indicating that both hurricanes drove mixing to deeper depths within the

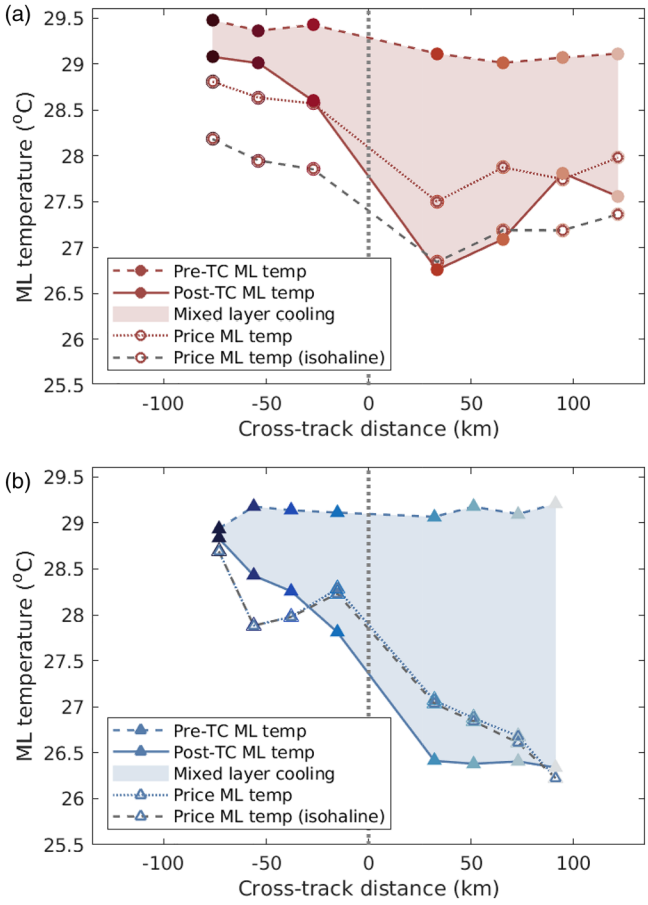

Figure 8. Temperature (°C) of the surface mixed layer at (a) Irma and (b) Florence ALAMO float locations, before (red and blue dashed) and after (solid) TC passage, and as diagnosed from the Price estimate using observed (dotted) and constant salinities (gray dashed). Shading highlights observed change in mixed layer temperature across each array. Radial distances (km, *x* axes) denote float locations at the TC CPA (as in Figure 3).

upper ocean. Cross-track differences in this maximum stratification are clear in the eyewall floats, where greater deepening is present right of the TC track than on the left. Radially outward from the eyewall floats, however, mixed layer deepening remains remarkably consistent (Figures 7a and 7b). Even though wind forcing at the surface decreases rapidly radially outward from the radius of maximum winds (e.g., by more than 80 kt on the right side of Irma), post-TC mixing extends to and oscillates about nearly the same depth (e.g., to about 100 m on the right side of Irma). Further, when comparing mean mixed layer depths at each location before (dashed red and blue lines, Figures 7c and 7d) and through three inertial periods after TC passage (except for 9140 which stopped reporting after about a day) across both arrays (solid lines, Figures 7c and 7d), we find that the mixed layer deepens (shaded regions, Figures 7c and 7d) an average of 50 m on the right side of each TC center, compared to less than 10 m on the left. These 40-m cross-track differences in hurricane-induced vertical mixing extent are generally consistent with results from previous studies (e.g., D'Asaro et al., 2007; Liu et al., 2019; Price, 1981). However, the similarities in mixed layer deepening with increasing distance from the radius of maximum winds to outer radii comprise a novel observation of this study. The location, magnitude, and extent of the cold wake this mixing creates drive changes in the air-sea enthalpy flux distribution and alter the surface atmospheric circulation (i.e., hurricane intensity).

While some of the disparity in Irma may be attributed to eyewall asymmetry (Figure 3) and/or differences in pre-TC salinities (and therefore densities, Figure 2) or even to the subsequent passage of Hurricane Jose (Figure 5), it is noteworthy that these cross-track differences were also present in Florence, where eyewall winds were nearly symmetric, pre-TC conditions were less variable, and a subsequent hurricane did not

overrun the array (Figures 2, 3, and 5). While direct cross-track and cross-storm comparisons need to be tempered with an awareness of differences in wind speeds and observation distances relative to the TC center, there is immense value in a comprehensive observational data set collected across two storms with similar radial-wind profiles over oceans with different initial conditions. Consistencies in these storm-forced ocean responses focus attention on dominant dynamical processes responsible for wake formation (mixing in this case) and highlight aspects of the upper ocean response that may be predictable.

4. Discussion

Price (2009, Equation 5) formulated an estimate of the depth that the surface mixed layer will reach when forced with a TC wind stress. We used his stability criterion to calculate the expected deepening of the surface mixed layer given the TC wind stress forcing. Specifically, the mixed layer is stable when it meets the following criterion:

$$\frac{g\,\delta\rho\,d}{\rho_0\,(\delta U)^2} \geq C,$$

where C is the critical bulk Richardson number, taken to be $C = 0.6$; g is the gravitational acceleration; $\delta\rho$ is the density difference between the surface and the depth of the mixed layer, d; ρ_0 is a reference density; and δU is the velocity shear between the surface and the base of the mixed layer. When the right-hand side is less than C, mixing will occur, and d will increase until this inequality is satisfied (as d increases, $\delta\rho$ will generally also increase, given a stably stratified ocean). Price (2009) then applied a further scaling argument (S; not shown), relating the velocity shear to the applied wind stress to enable estimation of mixing depth when subsurface current magnitudes are not available. Here, the velocity shear can be estimated from the float displacements, so the separate scaling argument and wind stress are not required. It is assumed that the bulk of the observed velocity is confined only to the upper ocean mixed layer, which appears to be reasonable based on previous observations of the surface mixed layer velocities in a hurricane (Sanford et al., 1987, 2007). It is also assumed that there is an insignificant velocity below the mixing layer, which the Ocean Surface Current Analyses Real-time data for the period prior to each TC passage support as well. Given those prerequisites, the integrated velocity transport, $\mathcal{T}$, over the profiling depth, D, is then equal to product of the slab mixed layer depth, d, and bulk velocity shear, δU (assuming the ocean velocity below the mixed layer is negligible), and results in the following relation:

$$\mathcal{T} = \int_0^D u(z)\,\mathrm{d}z \approx \delta U\,D \approx \delta U\,d,$$

where $u(z)$ is the ocean velocity as a function of the depth. Given the above stability criteria, along with the observed density as function of depth, $\rho(z)$, and the velocity shear, δU, from the maximum value of the float transport estimates, surface mixed layer deepening is estimated by solving for the depth that satisfies this stability criterion, represented in the following inequality:

$$d \geq \sqrt[3]{\frac{C\,\rho_0\,\mathcal{T}^2}{g\,\delta\rho}}.$$

The resulting estimated mixing depths reveal cross-track *differences* left and right of the TC centers and *similarities* from the radius of maximum winds to outer radii (dotted lines, Figures 7c and 7d). They also reflect differences between the TCs in intensity and near-surface density gradients and reasonably represent the approximate response observed across each track. While the Price formulation slightly overestimates the mixing left of track (by an average of 10 m in Florence and 20 m in Irma), the deepening right of track nearly matches the observations in both cases (differing by an RMS of less than 2 m in Florence and 8 m in Irma).

Interestingly, we can also use Price's formulation to evaluate the impact of salinity stratification on mixing depth across each TC track. We performed this mixing depth calculation for two cases: first for the actual observations (where density was determined from observed temperature, salinity, and pressure values) and, then to elucidate the impact of salinity, we calculated results using an isohaline profile (i.e., where

density was recomputed assuming a constant salinity = 35 PSU). In Florence, the estimated mixing depths are nearly identical (dashed gray and dotted blue lines, Figure 7d), which is understandable given the near-constant salinity values at those float locations. However, recomputing the mixing depth assuming a constant salinity profile shifts the mixing response dramatically along the Irma array. Without the very fresh surface layer, the poststorm mixing depth for Irma (dashed gray line, Figure 7c) would have been 20–30 m deeper than the full salinity estimate (dotted red line). This stronger mixing would have then fostered about 0.7°C of additional mixed layer cooling (Figure 8), which would have also errantly impacted surface fluxes and could have negatively impacted the accuracy of TC intensity forecasts. This result clearly identifies the impact salinity can have on upper ocean mixing and highlights the criticality of accurately characterizing both temperature and salinity within ocean models. Observations in areas with dynamic surface features, such as the Amazon-Orinoco River outflow region, are particularly important to correctly initialize coupled hurricane forecast models, and additional work is encouraged to further understand the impacts of salinity stratification on TC intensification (Hernandez et al., 2016; Rudzin et al., 2019).

One question raised by these observations is as follows: Why did such substantial and relatively uniform mixed layer deepening extend to such great distances from the radius of maximum winds, particularly right of the storm track? Resonance of the wind stress vector and local inertial frequency is known to factor into amplification of surface currents beneath TCs (e.g., Rayson et al., 2015; Samson et al., 2009) and could be one mechanism responsible for enhancing surface currents (and compensating for weaker wind speeds) at outer radii such that shear-driven entrainment yields consistent mixed layer deepening. Cross-track differences in resonance have been noted previously, for example, by Price (2009) who accounted for the asymmetry in his mixing parameterization with an ad hoc scaling constant of 0.4 left-of-track and 1.2 right-of-track. However, to the best of our knowledge, the radial dependence of that variability has not been observed in detail, and numerical studies are underway to further elucidate and quantify the effects of this mechanism on mixed layer deepening during hurricane passage.

5. Conclusions

We have described a comprehensive set of upper ocean measurements collected during the passage of two major hurricanes near maximum intensity and have discussed several results. In doing so, we have also highlighted the significance of the data set itself. The unique combination of horizontal, vertical, and temporal resolutions of these observations, along with corresponding surface wind and current estimates, offers three ways in which to advance understanding of the complex physical processes within and beneath major hurricanes.

First, the data set allows for investigation of known hypotheses based on less complete data sets and/or coupled ocean-atmosphere models. Our analysis of the Irma and Florence observations validates, quantifies, and extends results from previous studies as follows:

1. The ocean response to hurricane forcing is evident in sea surface cooling and in rapid deepening of upper ocean isotherms, isohalines, and isopycnals, followed by near-inertial oscillations of those contours in three dimensions. In both Irma and Florence, greatest ocean surface cooling (2.3°C and 2.4°C, respectively) was observed right of track shortly after TC passage. Below the surface, the 26°C isotherm plunged twice as far beneath the right eyewall (>20 m) than beneath the left (<10 m), and similar results extended radially outward from the radius of maximum winds.
2. Increased mixing is identified right of the TC center, characteristic of cross-track differences in upper ocean stability and mixing following hurricane passage. Of particular note, however, is the near-uniform magnitude of mixed layer deepening observed with increasing distance from each radius of maximum winds. In both storms, the mixed layer deepened nearly 50 m right of track compared to less than 10 m left of track, and in both cases, this deepening extended from the eyewall (under major hurricane winds) to outer radii where surface wind speeds reached only tropical storm intensities.
3. Salinity played a critical role in modulating upper ocean temperatures during hurricane passage. Differences in initial salinity stratification appear to have limited mixed layer deepening in Hurricane Irma and explain why the stronger winds in Irma resulted in weaker SST cooling. The impact of salinity on upper ocean mixing highlights an important link between salinity, surface fluxes, and changes in

hurricane intensity and points to the importance of accurately characterizing both temperature and salinity in coupled hurricane forecast models.

Next, the data set observations will be useful to address complex unresolved theoretical studies for which few observations exist, including air-sea heat exchange, heat and energy budgets, internal wave excitation and propagation, subsurface wake characteristics, and barrier layer studies. They support Price's (2009) scaling argument for how much of the upper ocean thermal energy is available to the TC as the upper ocean is mixed by the storm's winds and can be similarly used to verify other such parameterizations (e.g., Balaguru et al., 2018). They may also help refine and quantify the role of resonance in mixed layer deepening, particularly at extended distances from the radius of maximum winds right of the TC track.

Finally, the observations will enhance coupled numerical forecast models as they enable evaluation of model performance and parameterizations. Studies using these ALAMO float data are currently underway in the European Centre for Medium-Range Weather Forecasts and Coupled Ocean-Atmosphere Mesoscale Prediction System-Tropical Cyclone coupled numerical forecast models to test the fidelity of those models and identify deficiencies. Correcting model biases will lead to improvements in the model physics and ultimately to improved forecasts. Studies of these data are also underway by climate scientists analyzing wake persistence, quantifying ocean heat storage, and assessing the impacts of changing temperatures on the future of life in our oceans and on our planet.

Data Availability Statement

All float data are available online (http://argo.whoi.edu/alamo.html), and archived quality-controlled float data are available online (https://accession.nodc.noaa.gov/0210577). Additional data sources are listed in the supporting information.

Conflict of Interest

The authors declare no conflicts of interest relevant to this study.

Acknowledgments

The authors thank the U.S. Air Force Reserve 53rd Weather Reconnaissance Squadron for float deployment support. We thank Pelle Robbins and Alexander Ekholm (WHOI) and Sue Chen and James Cummings (NRL, Monterey, CA) for participation and support. We credit and appreciate Casey Densmore for assistance with final figure preparation and helpful comments on the manuscript. We are grateful to James Price, Patrick Harr, and Geoffrey Gebbie for fruitful conversations and constructive feedback. We also acknowledge Mark DeMaria and two anonymous reviewers whose valuable comments and critiques improved the manuscript. This work was supported by ONR Grants N0001416WX01262, N0001417WX01704, N0001418WX01452, and N000141812819 and NOAA Grants NA13OAR4830233 and NA14OAR4320158.

References

Androulidakis, Y., Kourafalou, V., Halliwell, G., Le Hénaff, M., Kang, H., Mehari, M., & Atlas, R. (2016). Hurricane interaction with the upper ocean in the Amazon-Orinoco plume region. *Ocean Dynamics, 66*, 1559–1588. https://doi.org/10.1007/s10236-016-0997-0

Balaguru, K., Foltz, G. R., Leung, L. R., Hagos, S. M., & Judi, D. R. (2018). On the use of ocean dynamic temperature for hurricane intensity forecasting. *Weather and Forecasting*, *33*, 411–418. https://doi.org/10.1175/WAF-D-17-0143.1

Bell, M. M., Montgomery, M. T., & Emanuel, K. A. (2012). Air–sea enthalpy and momentum exchange at major hurricane wind speeds observed during CBLAST. *Journal of the Atmospheric Sciences*, *69*, 3197–3222. https://doi.org/10.1175/JAS-D-11-0276.1

Bender, M. A., Marchok, T., Tuleya, R. E., Ginis, I., Tallapragada, V., & Lord, S. J. (2019). Hurricane model development at GFDL: A collaborative success story from a historical perspective. *Bulletin of the American Meteorological Society*, *100*, 1725–1736. https://doi.org/10.1175/BAMS-D-18-0197.1

Bhatia, K. T., Vecchi, G. A., Knutson, T. R., Murakarami, H., Kossin, J., Dixon, K. W., & Whitlock, C. E. (2019). Recent increases in tropical cyclone intensification rates. *Nature Communications*, *10*, 635. http://doi.org/10.1038/s41467-019-08471-z

Black, P. G., D'Asaro, E. A., Drennan, W. M., French, J. R., Niiler, P. P., Sanford, T. B., et al. (2007). Air-sea exchange in hurricanes: Synthesis of observations from the Coupled Boundary Layer Air-Sea Transfer experiment. *Bulletin of the American Meteorological Society*, *88*, 357–374. https://doi.org/10.1175/BAMS-88-3-357

Bonjean, F., & Lagerloef, G. S. E. (2002). Diagnostic model and analysis of the surface currents in the tropical Pacific Ocean. *Journal of Physical Oceanography*, *32*, 2938–2954. https://doi.org/10.1175/1520-0485(2002)032%3e2938:DMAAOT%3c2.0.CO;2

Cangialosi, J. P., Latto, A. S., & Berg, R. (2018). *Tropical cyclone report: Hurricane Irma (AL112017)* (Technical Report AL112017). Miami, FL: National Hurricane Center.

Chan, J. C. L., Duan, Y., & Shay, L. K. (2001). Tropical cyclone intensity change from a simple ocean–atmosphere coupled model. *Journal of the Atmospheric Sciences*, *58*, 154–172. https://doi.org/10.1175/1520-0469(2001)058%3e0154:TCICFA%3c2.0.CO;2

Chen, S., Cummings, J. A., Schmidt, J. M., Sanabia, E. R., & Jayne, S. R. (2017). Targeted ocean sampling guidance for tropical cyclones. *Journal of Geophysical Research: Oceans*, *122*, 3505–3518. https://doi.org/10.1002/2017JC012727

Chen, S., Elsberry, R. L., & Harr, P. A. (2017). Modeling interaction of a tropical cyclone with its cold wake. *Journal of the Atmospheric Sciences*, *74*, 3981–4001. https://doi.org/10.1175/JAS-D-16-0246.1

Cione, J. J., & Uhlhorn, E. (2003). Sea surface temperature variability in hurricanes: Implications with respect to intensity change. *Monthly Weather Review*, *131*, 1783–1796. https://doi.org/10.1175//2562.1

D'Asaro, E., Black, P. G., Centurioni, L. R., Chang, Y., Chen, S. S., Foster, R. C., et al. (2014). Impact of typhoons on the ocean in the Pacific. *Bulletin of the American Meteorological Society*, *95*, 1405–1418. https://doi.org/10.1175/BAMS-D-12-00104.1

D'Asaro, E. A., Sanford, T. B., Niiler, P. P., & Terrill, E. J. (2007). Cold wake of Hurricane Frances. *Geophysical Research Letters*, *34*, L15609. https://doi.org/10.1029/2007GL030160

Dare, R. A., & McBride, J. L. (2011). Sea surface temperature response to tropical cyclones. *Monthly Weather Review*, *139*, 3798–3808. https://doi.org/10.1175/MWR-D-10-05019.1

Edson, J. B., Jampana, V., Weller, R. A., Bigorre, S. P., Plueddemann, A. J., Fairall, C. W., et al. (2013). On the exchange of momentum over the open ocean. *Journal of Physical Oceanography*, *43*, 1589–1610. https://doi.org/10.1175/JPO-D-12-0173.1

Elsberry, R. L., Fraim, T. S., & Trapnell, R. N. (1976). A mixed layer model of the oceanic thermal response to hurricanes. *Journal of Geophysical Research*, *81*, 1153–1162. https://doi.org/10.1029/JC081i006p01153

Emanuel, K. A. (2005). Increasing destructiveness of tropical cyclones over the past 30 years. *Nature*, *436*, 686–688. https://doi.org/10.1038/nature03906

Ffield, A. (2007). Amazon and Orinoco River plumes and NBC Rings: Bystanders or participants in hurricane events? *Journal of Climate*, *20*, 316–333. https://doi.org/10.1175/JCLI3985.1

Fisher, E. L. (1958). Hurricanes and the sea surface temperature field. *Journal of Meteorology*, *15*, 328–333. https://doi.org/10.1175/1520-0469(1958)015%3e0328:HATSST%3c2.0.CO;2

Geisler, J. E. (1970). Linear theory of the response of a two layer ocean to a moving hurricane. *Geophysical Fluid Dynamics*, *1*, 249–272. https://doi.org/10.1080/03091927009365774

Gill, A. E. (1984). *Atmosphere-ocean dynamics*. London, UK: Academic Press.

Greatbatch, R. J. (1983). On the response of the ocean to a moving storm: The nonlinear dynamics. *Journal of Physical Oceanography*, *13*, 357–367. https://doi.org/10.1175/1520-0485(1983)013%3e0357:OTROTO%3c2.0.CO;2

Green, B. W., & Zhang, F. (2013). Impacts of air–sea flux parameterizations on the intensity and structure of tropical cyclones. *Monthly Weather Review*, *141*, 2308–2324. https://doi.org/10.1175/MWR-D-12-00274.1

Grodsky, S. A., Reul, N., Lagerloef, G., Reverdin, G., Carton, J. A., Chapron, B., et al. (2012). Haline hurricane wake in the Amazon/Orinoco plume: AQUARIUS/SACD and SMOS observations. *Geophysical Research Letters*, *39*, L20603. https://doi.org/10.1029/2012GL053335

Halliwell, G. R., Gopalakrishnan, S., Marks, F., & Willey, D. (2015). Idealized study of ocean impacts on tropical cyclone intensity forecasts. *Monthly Weather Review*, *143*, 1142–1165. https://doi.org/10.1175/MWR-D-14-00022.1

Hernandez, O., Jouanno, J., & Durand, F. (2016). Do the Amazon and Orinoco freshwater plumes really matter for hurricane-induced ocean surface cooling? *Journal of Geophysical Research: Oceans*, *121*, 2119–2141. https://doi.org/10.1002/2015JC011021

Hidaka, K., & Akiba, Y. (1955). Upwelling induced by a circular wind system. *Records of Oceanographic Works in Japan*, *2*, 7–18.

Hlywiak, J., & Nolan, J. (2019). The influence of oceanic barrier layers on tropical cyclone intensity as determined through idealized, coupled numerical simulations. *Journal of Physical Oceanography*, *49*, 1723–1745. https://doi.org/10.1175/JPO-D-18-0267.1

Holland, G., & Bruyère, C. L. (2014). Recent intense hurricane response to global climate change. *Climate Dynamics*, *42*, 617–627. https://doi.org/10.1007/s00382-013-1713-0

Jayne, S. R., & Bogue, N. M. (2017). Air-deployable profiling floats. *Oceanography*, *30*(2), 29–31. https://doi.org/10.5670/oceanog.2017.214

Lee, C. Y., & Chen, S. S. (2014). Stable boundary layer and its impact on tropical cyclone structure in a coupled atmosphere–ocean model. *Monthly Weather Review*, *142*, 1927–1944. https://doi.org/10.1175/MWR-D-13-00122.1

Leipper, D. F. (1967). Observed ocean conditions and Hurricane Hilda, 1964. *Journal of the Atmospheric Sciences*, *24*, 182–186. https://doi.org/10.1175/1520-0469(1967)024%3e0182:OOCAHH%3c2.0.CO;2

Lin, I. I. (2012). Typhoon-induced phytoplankton blooms and primary productivity increase in the western North Pacific subtropical ocean. *Journal of Geophysical Research*, *117*, C03039. https://doi.org/10.1029/2011JC007626

Liu, X., Wei, J., Zhang, D.-L., & Miller, W. (2019). Parameterizing sea surface temperature cooling induced by tropical cyclones: 1. Theory and an application to Typhoon Matsa (2005). *Journal of Geophysical Research: Oceans*, *124*, 1215–1231. https://doi.org/10.1002/2018JC014118

Mogensen, K. S., Magnusson, L., & Bidlot, J. R. (2017). Tropical cyclone sensitivity to ocean coupling in the ECMWF coupled model. *Journal of Geophysical Research: Oceans*, *122*, 4392–4412. https://doi.org/10.1002/2017JC012753

Mrvalijevic, R. K., Black, P. G., Centurioni, L. R., Chang, Y.-T., D'Asaro, E. A., Jayne, S. R., et al. (2013). Observations of the cold wake of Typhoon Fanapi (2010). *Geophysical Research Letters*, *40*, 316–321. https://doi.org/10.1029/2012GL054282

Murakami, H., Levin, E., Delworth, T. L., Gudgel, R., & Hsu, P. C. (2018). Dominant effect of relative tropical Atlantic warming on major hurricane occurrence. *Science*, *362*, 794–799. https://doi.org/10.1126/science.aat6711

Price, J. F. (1981). Upper ocean response to a hurricane. *Journal of Physical Oceanography*, *11*, 153–175. https://doi.org/10.1175/1520-0485(1981)011%3e0153:UORTAH%3c2.0.CO;2

Price, J. F. (1983). Internal wave wake of a moving storm. Part I: Scales, energy budget and observations. *Journal of Physical Oceanography*, *13*, 949–965. https://doi.org/10.1175/1520-0485(1983)013%3e0949:IWWOAM%3c2.0.CO;2

Price, J. F. (2009). Metrics of hurricane-ocean interaction: Vertically-integrated or vertically-averaged ocean temperature? *Ocean Science*, *5*, 351–368. https://doi.org/10.5194/os-5-351-2009

Price, J. F., Sanford, T. B., & Forristall, G. Z. (1994). Forced stage response to a moving hurricane. *Journal of Physical Oceanography*, *24*, 233–260. https://doi.org/10.1175/1520-0485(1994)024%3e0233:FSRTAM%3c2.0.CO;2

Rayson, M. D., Ivey, G. N., Jones, N. L., Lowe, R. J., Wake, G. W., & McConochie, J. D. (2015). Near-inertial ocean response to tropical cyclone forcing on the Australian North-West Shelf. *Journal of Geophysical Research: Oceans*, *120*, 7722–7751. https://doi.org/10.1002/2015JC010868

Rudzin, J. E., Shay, L. K., & de la Cruz, B. J. (2019). The impact of the Amazon–Orinoco River Plume on enthalpy flux and air–sea interaction within Caribbean Sea tropical cyclones. *Monthly Weather Review*, *147*, 931–950. https://doi.org/10.1175/MWR-D-18-0295.1

Rudzin, J. E., Shay, L. K., & Johns, W. E. (2018). The influence of the barrier layer on SST response during tropical cyclone wind forcing using idealized experiments. *Journal of Physical Oceanography*, *48*, 1471–1478. https://doi.org/10.1175/JPO-D-17-0279.1

Samson, G., Giordani, H., Caniaux, G., & Roux, F. (2009). Numerical investigation of an oceanic resonant regime induced by hurricane winds. *Ocean Dynamics*, *59*, 565–586. https://doi.org/10.1007/s10236-009-0203-8

Sanford, T. B., Black, P. G., Haustein, J. R., Feeney, J. W., Forristall, G. Z., & Price, J. F. (1987). Ocean response to a hurricane. Part I: Observations. *Journal of Physical Oceanography*, *17*, 2065–2083. https://doi.org/10.1175/1520-0485(1987)017%3e2065:ORTAHP%3c2.0.CO;2

Sanford, T. B., Price, J. F., & Girton, J. B. (2011). Upper-ocean response to Hurricane Frances (2004) observed by profiling EM-APEX floats. *Journal of Physical Oceanography*, *41*, 1041–1056. https://doi.org/10.1175/2010JPO4313.1

Sanford, T. B., Price, J. F., Girton, J. B., & Webb, D. C. (2007). Highly resolved observations and simulations of the ocean response to a hurricane. *Geophysical Research Letters*, *34*, L13604. https://doi.org/10.1029/2007GL029679

Shay, L. K., Black, P. G., Mariano, A. J., Hawkins, J. D., & Elsberry, R. L. (1992). Upper ocean response to hurricane Gilbert. *Journal of Geophysical Research*, *97*, 20,227–20,248. https://doi.org/10.1029/92JC01586

Sriver, R. L., & Huber, M. (2007). Observational evidence for an ocean heat pump induced by tropical cyclones. *Nature*, *447*, 577–580. https://doi.org/10.1038/nature05785

Stewart, S. R., & Berg, R. (2019). *Tropical cyclone report: Hurricane Florence (AL062018)* (Technical report AL062018). Miami, FL: National Hurricane Center.

Stramma, R. S., Cornillon, P., & Price, J. F. (1986). Satellite observation of sea surface cooling by hurricanes. *Journal of Geophysical Research*, *91*, 5031–5035. https://doi.org/10.1029/JC091iC04p05031

Suda, K. (1943). *The science of the sea (Kaiyō Kagaku)*. Tokyo, Japan: Kokin Shoin.

Uhlhorn, E. W., Black, P. G., Franklin, J. L., Goodberlet, M., Carswell, J., & Goldstein, A. S. (2007). Hurricane surface wind measurements from an operational Stepped Frequency Microwave Radiometer. *Monthly Weather Review*, *135*, 3070–3085. https://doi.org/10.1175/MWR3454.1

Walker, N. D., Leben, R. R., & Balasubramanian, S. (2005). Hurricane-forced upwelling and chlorophyll *a* enhancement within cold-core cyclones in the Gulf of Mexico. *Geophysical Research Letters*, *32*, L18610. https://doi.org/10.1029/2005GL023716

Wang, X., Han, G., Qi, Y., & Li, W. (2011). Impact of barrier layer on typhoon-induced sea surface cooling. *Dynamics of Atmospheres and Oceans*, *52*, 367–385. https://doi.org/10.1016/j.dynatmoce.2011.05.002

Wentz, F. J., Gentemann, C., Smith, D., & Chelton, D. (2000). Satellite measurements of sea surface temperature through clouds. *Science*, *228*, 847–850. https://doi.org/10.1126/science.288.5467.847

Zhu, H., Ulrich, W., & Smith, R. K. (2004). Ocean effects on tropical cyclone intensification and inner-core asymmetries. *Journal of the Atmospheric Sciences*, *61*, 1245–1258. https://doi.org/10.1175/1520-0469(2004)061%3e1245:OEOTCI%3c2.0.CO;2

References From the Supporting Information

Fofonoff, N. P., & Millard Jr., R. C. (1983). Algorithms for computation of fundamental properties of seawater. *UNESCO Technical Papers in Marine Science, 44*. https://hdl.handle.net/1912/2470

Halverson, M., Siegel, E., & Johnson, G. (2020). Inductive-conductivity cell. *Sea Technology*, *61*(2), 24–27. https://www.sea-technology.com